1   Comparison of climatological planetary boundary layer depth estimates using the GEOS-5

2   AGCM

3   Erica L. McGrath-Spangler

4   Universities Space Research Association

5   10211 Wincopin Circle, Suite 500 Columbia, MD 21044

6   and

7   Global Modeling and Assimilation Office, Code 610.1

8   NASA Goddard Space Flight Center

9   8800 Greenbelt Rd.

10   Greenbelt, MD 20771

11

12   Andrea Molod

13   Earth System Sciences Interdisciplinary Center

14   University of Maryland

15   College Park, MD 20740

16   and

17   Global Modeling and Assimilation Office, Code 610.1

18   NASA Goddard Space Flight Center

19   8800 Greenbelt Rd.

20   Greenbelt, MD 20771

21

22   E. L. McGrath-Spangler   301-614-5838   erica.l.mcgrath-spangler@nasa.gov

23   A. Molod   301-614-6845   andrea.m.molod@nasa.gov

1

24

25   Abstract

26   Planetary boundary layer (PBL) processes, including those influencing the PBL depth,

27   control many aspects of weather and climate and accurate models of these processes are

28   important for forecasting changes in the future. However, evaluation of model estimates of PBL

29   depth are difficult because no consensus on PBL depth definition currently exists and various

30   methods for estimating this parameter can give results that differ by hundreds of meters or more.

31   In order to facilitate comparisons between the Goddard Earth Observation System (GEOS-5) and

32   other modeling and observational systems, seven PBL depth estimation methods are used to

33   produce PBL depth climatologies and are evaluated and compared here. All seven methods

34   evaluate the same atmosphere so all differences are related solely to the definition chosen. These

35   methods depend on the scalar diffusivity, bulk and local Richardson numbers, and the diagnosed

36   horizontal turbulent kinetic energy (TKE). Results are aggregated by climate class in order to

37   allow broad generalizations.

38   The various PBL depth estimations give similar midday results with some exceptions.

39   One method based on horizontal turbulent kinetic energy produces deeper PBL depths in the

40   winter associated with winter storms. In warm, moist conditions, the method based on a bulk

41   Richardson number gives results that are shallower than those given by the methods based on the

42   scalar diffusivity. The impact of turbulence driven by radiative cooling at cloud top is most

43   significant during the evening transition and along several regions across the oceans and methods

44   sensitive to this cooling produce deeper PBL depths where it is most active. Additionally,

45   Richardson number-based methods collapse better at night than methods that depend on the

46   scalar diffusivity. This feature potentially affects tracer transport.

1.   Introduction

The planetary boundary layer (PBL) is crucial to surface-atmosphere exchanges of momentum, energy, moisture, aerosols, carbon, and other chemical tracers. Accurately modeling the PBL character and height in global atmospheric general circulation models (AGCMs) has significant implications for climate and weather predictions, and is made difficult due to the lack of adequate observations. The depth of this layer, in particular, is important for air quality studies since pollutants, aerosols, and carbon dioxide that are emitted near the surface are turbulently mixed throughout the layer and the depth reflects the amount and profile of the turbulence. Inversion studies, which seek to estimate surface fluxes given surface concentrations, are explicitly sensitive to PBL depth errors in atmospheric models [*Gurney et al.*, 2002].

The PBL parameterization is flawed in many numerical weather models and this leads to prediction errors [*Beljaars*, 1995; *Joffre et al.*, 2001]. These flaws, combined with only limited measurements, contribute to the difficulty of producing a PBL depth comprehensive climatology, despite its importance [*Joffre et al.*, 2001]. In addition, multiple PBL depth definitions exist and these can give different results [*Seidel et al.*, 2010], complicating PBL depth estimation and comparisons between models and observations.

Several studies have attempted to understand the uncertainty associated with the use of different PBL depth definitions and found the result to depend substantially on the method chosen. *Vogelezang and Holtslag* [1996] examined the PBL depth by defining it using both bulk and gradient Richardson numbers and found that the choice of Richardson number, the critical number chosen, and the inclusion of surface friction impacted the results. *White et al.* [1999] used summertime data near Nashville, Tennessee to compare the PBL depth estimated by wind

70 profilers and an airborne differential absorption lidar (DIAL). They found that the different

71 datasets produced similar PBL depths under clear conditions (correlation coefficient of 0.94 and

72 mean offset of 37 m), but the agreement degraded under cloudy conditions (correlation

73 coefficient of 0.87) with a mean difference of about 150 meters.

74   *Seibert et al.* [2000] found that all PBL height definition schemes had deficiencies under

75 certain conditions. They examined 7 different datasets and 10 equations commonly used to

76 determine the PBL depth and concluded that the definitions have to be seen in the context of the

77 data used. Likewise, *Seidel et al.* [2010] tested 7 different PBL depth definition methods on

78 radiosonde profiles. Using a single dataset, the estimated PBL depth was found to generally

79 differ by several hundred meters, depending on the method used. The use of different methods

80 in their study produced differences of more than 1 km and even produced different seasonal

81 variations. These differences were statistically significant in practically all comparisons between

82 methods, introducing a structural uncertainty of 10-100% of climatological means. *Seidel et al.*

83 [2010] concluded that it is necessary to compare different PBL depth estimates using the same

84 method. They suggested the development of multiple climatologies using different definitions

85 and the use of the appropriate one for the application desired.

86   In the present study, seven different methods to compute the PBL depth, based on vertical

87 profiles of the scalar diffusivity, the bulk and local Richardson (Ri) numbers, and the horizontal

88 component of the turbulent kinetic energy (TKE), are incorporated into the Goddard Earth

89 Observation System (GEOS-5) AGCM [*Rienecker et al.*, 2008; *Molod et al.*, 2012] and

90 compared using a single climate simulation. In order to provide insight into implications on the

91 regional and global climate scale, results are aggregated using Köppen-Geiger climate classes

92 [*Peel et al.*, 2007].

4

93   The purpose of this study is two-fold. First, it analyzes differences among the PBL depth

94   definitions within the GEOS-5 model using the same atmosphere. Second, it enables a

95   comparison among GEOS-5, observations, and other numerical simulations using the same

96   definition so as to evaluate the atmospheric profiles rather than the method used.

97   The following section provides a model description and a description of the PBL depth

98   diagnostics used. The third section presents results, and the final section contains the

99   conclusions.

100   2.   Model and PBL Diagnostics

101   2.1   GEOS-5 Model Description

102   The GEOS-5 AGCM is part of the GEOS-5 data assimilation system, an earlier version

103   of which was used for the Modern-Era Retrospective Analysis for Research and Applications

104   (MERRA) [*Rienecker et al.*, 2011]. The latitude-longitude hydrodynamical core of GEOS-5

105   uses the finite volume dynamical core of *Lin* [2004] and the cubed sphere version is based on

106   *Putman and Lin* [2007]. GEOS-5 includes moist physics with prognostic clouds [*Bacmeister et*

107   *al.*, 2006]. The convective scheme is a modified version of the Relaxed Arakawa-Schubert of

108   *Moorthi and Suarez* [1992], the shortwave radiation scheme is that of *Chou and Suarez* [1999],

109   and *Chou et al.* [2001] describe the longwave radiation scheme. The Catchment Land Surface

110   Model is used to determine fluxes at the land/atmosphere interface [*Koster et al.*, 2000] and the

111   surface layer is determined as in *Helfand and Schubert* [1995]. The model uses 72 vertical

112   pressure layers that transition from terrain following near the surface to pure pressure levels

113   above 180 hPa [*Rienecker et al.*, 2008; *Molod et al.*, 2012] and this study uses approximately ½

114   degree horizontal resolution on the cubed sphere. The simulation covers January 1990 through

115   May 2013.

116   GEOS-5 includes two atmospheric boundary layer turbulent mixing schemes [*Rienecker*

117   *et al.*, 2008]. The scheme of *Louis et al.* [1982] is used in conjunction with the scheme of *Lock*

118   *et al.* [2000]. The Lock scheme is a non-local first order scheme in which the diffusivities are

119   computed based on the buoyancy associated with the surface based (positive buoyancy) and the

120   cloud-based radiative cooling (negative buoyancy) "plumes". This scheme has been extended in

121   GEOS-5 so that the unstable surface plume calculation includes moist heating and entrainment

122   [*Rienecker et al.*, 2008]. The Louis scheme is a first order local scheme in which the turbulence

123   diffusivities are computed as functions of the gradient Richardson number. The turbulent length

124   scale is assumed to be related to the PBL height as diagnosed from the Louis-Lock combined

125   eddy diffusivities. The eddy diffusivities used for the AGCM turbulent diffusion are the larger

126   of the Lock or Louis diffusivities at any time step [*Molod et al.*, 2012].

127   2.2   PBL Depth Diagnostics

128   Seven different methods for determining the PBL depth are evaluated using the GEOS-5

129   model based on several different output variables (Table 1). All methods evaluate the same

130   atmospheric profiles and all differences are related solely to the choice of definition. The PBL

131   depth based on the total scalar diffusivity using method 1, is used to compute the turbulent length

132   scale [*Blackadar*, 1962] for the Louis scheme. This PBL depth is termed "active" since it feeds

133   back to the turbulence scheme and determines the vertical extent of mixing. This first method

134   estimates the PBL depth as the model level above which the scalar diffusivity falls below a

135   threshold value of 2 $m^2\,s^{-1}$.

136   The use of the scalar diffusivity to define the PBL depth is further investigated by using a

137   threshold of 10% of the column maximum and linearly interpolating between levels to determine

138   the PBL depth. Method 2 uses the total scalar diffusivity and method 3 uses the surface

139   buoyancy driven scalar diffusivity, but neglects the radiatively driven component defined by the

140   *Lock et al.* [2000] scheme.

141   The PBL depth definition used by *Seidel et al.* [2012] and based on the work by

142   *Vogelezang and Holtslag* [1996] is used as the fourth method. *Seidel et al.* [2012] selected this

143   method because of its applicability to radiosondes and model simulations and its suitability for

144   convective and stable boundary layers. This method uses a bulk Richardson number given by:

145    $Ri_b(z) = \dfrac{(\frac{g}{\theta_{vz}})(\theta_{vz} - \theta_{vs})(z - z_s)}{u_z^2 + v_z^2}$

146   Ri_b is the Richardson number, g is gravity, θ_v is the virtual potential temperature, u and v are the

147   horizontal wind components, and z is height. The subscript s denotes the surface and the surface

148   winds are assumed zero. The Richardson number is evaluated between the surface and

149   successively higher heights, identifying the PBL top as the level at which Ri exceeds a critical

150   value of 0.25. The PBL height is found by linearly interpolating between model levels.

151   Additionally, two other methods use a different version of the Richardson number evaluated

152   between two consecutive levels rather than between the surface and the current height. These

153   methods use a local Richardson number calculated as:

154    $Ri(z) = \dfrac{(\frac{g}{\theta_v})(\theta_{vz1} - \theta_{vz2})(z1 - z2)}{(u_{z1} - u_{z2})^2 + (v_{z1} - v_{z2})^2}$

155   Here, $z2$ represents the level height below the height z1 and θ_v without a subscript is the average

156   virtual potential temperature between heights $z1$ and $z2$. The fifth method tests a critical

157   Richardson number value of 0 and the sixth tests a critical value of 0.2.

158   Finally, since the PBL is generally considered turbulent with only sporadic clear air

159   turbulence aloft [*Stull*, 1988], the TKE due to shear is used to estimate the PBL depth in the

160   seventh method. The horizontal TKE is estimated from the wind shear and momentum

161 diffusivity and then the top of the PBL is taken to be the height at which the value falls below a

162 threshold value of 10% of the column maximum.

163 2.3   Climate Classes

164   *Peel et al.* [2007] recently updated the Köppen-Geiger climate classification, taking

165 advantage of advances in data availability and computing power. They did this by using monthly

166 mean precipitation and temperature data from over 4000 stations (plus additional data from

167 stations reporting only temperature or only precipitation) and interpolating between them using a

168 two-dimensional thin-plate spline with tension. The final map is generated on a 0.1°x0.1° grid.

169 The highest station density is in the USA, southern Canada, northeast Brazil, Europe, India,

170 Japan, and eastern Australia while the lowest station data is located in desert, polar, and some

171 tropical regions.

172   *Peel et al.* [2007] used the same classes as the original classification system, but with an

173 updated boundary condition between the temperate and cold climate classes. The classification

174 consists of five main classes consisting of tropical (A), arid (B), temperate (C), cold (D), and

175 polar (E) with further divisions based on seasonal variations in temperature and precipitation.

176 *Peel et al.* [2007] provides a full description of the climate classifications including details on

177 how the classification was determined. The broad climate types are relatively insensitive to

178 temperature trends, including those from global climate change [*Triantafyllou and Tsonis*, 1994;

179 *Peel et al.*, 2007] and are intended to represent long term mean climate conditions and not year-

180 to-year variability.

181   In an effort to generalize the results of this analysis, the computed PBL depths are

182 aggregated by season onto the Köppen-Geiger climate classes, which are regridded to the 1/2°

183 horizontal grid used by GEOS-5 (Figure 1). The Köppen-Geiger climate classes have been used

184 to group rivers worldwide for comparisons of runoff characteristics [*McMahon et al.*, 1992; *Peel*

185 *et al.*, 2004]. Similarly, *Molod and Salmun* [2002] successfully used this technique in their study

186 investigating the implications of using different land surface modeling approaches. Their study

187 aggregated results such as canopy temperature, soil moisture, and turbulent fluxes and they were

188 able to use these results to make generalizations that extend to broad climate regions relevant for

189 global models. These climate classes are a way to characterize similar remote regions and apply

190 findings globally. However, it is important to keep in mind that this classification does not take

191 into account other aspects of the climate system relevant to boundary layer processes.

192 Differences such as intensity of precipitation, elevation, and overlying subsidence are not

193 considered.

194 3.   Results

195 3.1   Regimes within Climate Classes

196   The Köppen-Geiger climate classes organize remote land regions together based on

197 temperature and precipitation. However, these regions can have very different large-scale

198 dynamics that also influence the PBL depth such as subsidence, intensity and frequency of

199 precipitation, and terrain. Two examples of this type of variability within climate classes are

200 presented here. The first example is illustrated in Figure 2, which shows the climatological

201 relationship between PBL depth and sensible heat flux for climate class BWh (arid, hot desert) in

202 winter. Each point on the scatter plot represents the seasonal mean midday PBL depth and

203 sensible heat flux for a GEOS-5 grid cell within the BWh climate class.

204   Several different regimes are present associated with different climatic conditions. The

205 Australian deserts (the non-black points, colored according to evaporative fraction), in particular,

206 have two different regimes associated with them during the winter. The first regime at low

9

207 sensible heat flux (<100 W m^{-2}) is associated with evaporative fractions above 0.3 while the

208 other regime, characterized by sensible heat fluxes between 100 and 260 W m^{-2} and shallower

209 PBL depths, has evaporative fractions around 0.2. This second regime has less variation of PBL

210 depths with sensible heat, and has a median depth about 260 meters shallower than the first

211 regime. This shows that similar climate and physical proximity cannot explain all PBL depth

212 variability.

213   The second example is illustrated in Figure 3, which shows the relationship between PBL

214 depth and 10-meter temperature for the tropical rainforest climate class (Af) colored according to

215 relative humidity. In this climate class and the other tropical climate classes, there is a shift in

216 the relationship occurring around 302 K. This temperature is near the wilting point for broadleaf

217 evergreen, the dominant vegetation type in the tropics. At temperatures above the wilting point,

218 the vegetation experiences stress thus severely limiting transpiration and near surface humidity.

219 In these drier conditions, less energy goes in to evaporating water and, by energy balance, more

220 goes in to sensible heat flux. Since sensible heat is much more efficient at growing the PBL than

221 latent heat, the PBL depth increases rapidly with temperature in this drier regime [*Avissar and*

222 *Pielke*, 1989]. In the regime below the wilting point, transpiration increases with temperature

223 and proceeds with little resistance, wetting the lower atmosphere. In this wetter regime, PBL

224 depth decreases with temperature.

225   These different regimes and sensitivities of PBL depth to different variables must be kept

226 in mind when examining climatological boundary layer depth. Although the Köppen-Geiger

227 climate classes are able to capture a lot of the variability and are useful for organizing land

228 regions in order to make generalizations and simplify the analysis, they do not capture all the

229 large-scale climate conditions relevant to boundary layer processes. There will therefore be

230   geographical differences between regions within a climate class that will not be captured by this

231   analysis.

232   3.2   General Method Behavior

233   Generally, the PBL depth definitions produce similar results. Differences are highlighted

234   below. Figure 4 shows the seasonal mean diurnal cycle for the cold climate class with dry, hot

235   summer (Dsa during summer 4a and winter 4c) and hot, arid desert (BWh during summer 4b and

236   winter 4d). For these climate classes, the scalar diffusivity methods using a 10% threshold

237   (methods 2 and 3) are insensitive to the use of the radiative plume from the Lock turbulence

238   scheme. The PBL depths estimated using the bulk Richardson number (method 4), the TKE

239   (method 7), and the three scalar diffusivity methods (methods 1, 2, and 3) give comparable

240   midday results over land, giving us confidence in the estimated depth under these conditions.

241   Although the horizontal TKE definition gives similar midday results to the scalar

242   diffusivity and bulk Richardson number methods under most conditions, during the winter in

243   temperate and cold climates, the horizontal TKE method often gives PBL depths that are 100

244   meters or more deeper than the other methods (Figure 4c and 4d). This is due to the winter storm

245   tracks and associated increase in wind shear. The horizontal TKE is diagnosed in the model by

246   multiplying the momentum diffusivity by the local wind shear making the horizontal TKE

247   method more sensitive to the wind profile and seasonal changes to it than the other methods.

248   The stronger and deeper wind shear thus produces a deeper turbulent layer and therefore a deeper

249   diagnosed PBL depth based on this variable.

250   The results from the horizontal TKE method, while consistent with other PBL methods

251   over land, are inconsistent with the other methods over the oceans. The horizontal TKE derived

252   PBL depth gives results as much as 400 meters deeper than the other definitions and have diurnal

253 variability considerably larger. It is therefore suggested that this method not be used to estimate

254 marine boundary layer depths.

255 The methods based on the local Richardson number estimate PBL depths that are several

256 hundred meters shallower at midday than PBL depths using the other methods. This method

257 does not depend greatly on the critical Richardson number chosen as the differences between

258 PBL depths estimated using a critical value of zero are only slightly shallower than PBL depths

259 estimated using a critical value of 0.2. *Seidel et al.* [2012] similarly found small uncertainty

260 associated with the choice of critical value in their study.

261 The Richardson number based methods (local and bulk) collapse better at night than the

262 definitions based on the scalar diffusivity or TKE. This has implications for estimating the

263 shallow nocturnal boundary layer and studies involving tracer transport. For instance, over

264 climate class BWh (arid, hot desert representing such areas as the Sahara and Australian deserts,

265 Figure 4b), the bulk Richardson number nocturnal PBL is well under 500 meters and the local

266 Richardson number PBL depths are only a few hundred meters while the scalar diffusivity

267 methods estimate a PBL depth between 1000 and 1500 meters at night during the summer.

268 3.3   Bulk Richardson vs. Scalar Diffusivity Methods

269 While the bulk Richardson number and scalar diffusivity methods generally give similar

270 midday results, under warm, wet conditions, the estimated daily maximum PBL depth found

271 using the bulk Richardson number method tends to be shallower than the scalar diffusivity

272 methods. This occurs for the tropical rainforest climate class (Figure 5) as well as the other

273 tropical climate classes during their rainy seasons and even for temperate climate classes when it

274 is both warm and there is a lot of precipitation. This difference means that the Richardson

275 number exceeds its critical value at a level below which the scalar diffusivity decreases to its

276 threshold value. This implies a virtual potential temperature inversion occurring within the

277 layer of relatively high scalar diffusivity. Figure 6 shows the June, July, and August (JJA)

278 seasonal mean vertical profiles of total scalar diffusivity, the scalar diffusivity from the Louis

279 parameterization, and the Richardson number from a typical location within the Amazonian

280 rainforest. The horizontal dashed lines indicate the PBL depth found using the total scalar

281 diffusivity (method 1, Figure 6a) and Richardson number (method 4, Figure 6b). These profiles

282 show that the Richardson number becomes stable below where the scalar diffusivity declines.

283 This could occur under several different meteorological conditions. There could be a

284 turbulent layer aloft that is not fully decoupled from the surface layer that is being detected by

285 the scalar diffusivity methods, but not the bulk Richardson number method. If the scalar

286 diffusivity predicted by the Louis scheme (Figure 6a) is shallow with its maximum low to the

287 ground, it can be expected that the PBL depth found using the bulk Richardson number might

288 also be shallow. The Louis turbulence parameterization is dependent upon a local Richardson

289 number and so contains some information about the vertical profile of temperature and shear.

290 While this is a different form of the Richardson number from what is used in the bulk

291 Richardson number method, the Louis scheme can provide information about what to expect

292 from the bulk Richardson number method. If, however, the Lock scheme is strongly active aloft

293 due to entrainment or radiation, the scalar diffusivity methods may detect a deeper PBL.

294 3.4   Impact of radiative plume

295 The Lock turbulence scheme extends the nonlocal eddy-viscosity based scheme based on

296 *Holtslag and Boville* [1993] to include the effects of radiative cooling at cloud top by positing a

297 turbulent "radiative plume" descending from cloud base due to negative buoyancy associated

298 with radiative cooling. In order to test the impact of the associated radiative plume, the scalar

299   diffusivity method using a threshold of 10% of the column maximum was tested both with

300   (method 2) and without (method 3) the scalar diffusivity associated with the radiative plume.

301   Figure 7 shows the diurnal cycle of the PBL depth difference between the two methods for JJA.

302   At all locations, the PBL depth estimated using the radiative plume was deeper or the same

303   height as that without the plume. The largest differences occurred over land in the summer

304   hemisphere and in the tropics during the evening transition. This result holds for December,

305   January, and February (DJF) as well (not shown). The evening timing is because the radiative

306   plume is sensitive to cloud top. At night, the scalar diffusivities decrease due to the lack of

307   incoming solar radiation, but the diffusivity associated with the radiative plume decreases less

308   proportionally to the other diffusivities since the cloud does not dissipate during the evening

309   transition. The radiative plume scalar diffusivity thus becomes proportionally more important at

310   night and the PBL depth remains deeper. The non-radiative method therefore collapses better at

311   night.

312   In addition to the maxima over land, there are persistent regions of relatively large

313   radiative plume impact over the oceans around 30°N and 45°S. This is due to the way GEOS-5

314   estimates the effective liquid cloud particle radius. GEOS-5 uses an empirical model based on

315   temperature, pressure, and wind speed to estimate this radius. The large differences over oceans

316   are located in regions with a temperature transition, creating a collocation of relatively small

317   prescribed effective radii and boundary layer clouds. In cloudy regions, more shortwave

318   radiation is absorbed in areas with many small droplets than in areas with fewer large droplets.

319   This produces an increase in temperature leading to an enhanced longwave flux, which drives the

320   radiative plume. Since the radiative plume is more active in these locations, PBL methods

321   sensitive to its impact are deeper than if the radiative plume was neglected.

322   4.   Conclusions

323   Although the PBL depth is important for AGCMs and has implications for climate and

324   weather prediction, observations are limited and no consensus on definition exists. Complicating

325   things further, under certain conditions, different definitions can give significantly different

326   results. This study examines this issue by using seven different methods to define the PBL depth

327   using the same atmosphere so that all differences can be attributed directly to the definition. It

328   is, however, important to point out that this is not an extensive validation. Results are

329   aggregated to Köppen-Geiger climate classes in order to make broad generalizations and

330   simplify the analysis on a global scale. Within these climate classes, different regimes are

331   present that are related to differences in temperature and evaporative fraction. These differences

332   are not captured when the results are aggregated, but the general behavior is represented.

333   Under most conditions, the bulk Richardson number, scalar diffusivity, and horizontal

334   TKE methods give similar midday results over land. The horizontal TKE definition is more

335   sensitive to winter storms and their associated shear and so estimate deeper midday PBL depths

336   during the winter season. The local Richardson number methods are relatively insensitive to the

337   critical Richardson number used and estimate PBL depths several hundred meters shallower than

338   the other methods. Both the local and bulk Richardson number methods collapse better at night

339   than the scalar diffusivity and TKE methods. For instance, over hot, arid deserts, the bulk

340   Richardson number method estimates a nocturnal PBL depth that is up to a kilometer shallower

341   than the default scalar diffusivity method using a threshold of $2 \mathrm{\ m^2\,s^{-1}}$.

342   Under warm, moist conditions, the bulk Richardson number method estimates PBL

343   depths that are shallower than those estimated by the scalar diffusivity methods. This indicates

344   that the Richardson number is exceeding its threshold value below the level at which the scalar

15

345   diffusivity decreases to its threshold value. This response is associated with a maximum in the

346   Louis scheme scalar diffusivity near the surface and Lock scheme scalar diffusivities with

347   maxima higher in the atmosphere.

348   The Lock scheme includes the effects of a radiative plume associated with longwave

349   cloud base cooling. The impact of this effect on PBL depth was found to have its strongest

350   effect over land during the evening transition because of the persistence of cloud cover through

351   the diurnal cycle. Additionally, regions of influence were found in the marine boundary layer

352   related to the way the effective liquid cloud radius is defined in GEOS-5.

353   This study analyzes the sensitivity of the PBL depth in GEOS-5 to the definition chosen

354   under different meteorological conditions. Although each definition was evaluated using

355   identical atmospheres, under various environments the resulting PBL depth could differ by a

356   kilometer or more. This reinforces the recommendation by *Seidel et al.* [2010] that PBL depths

357   be compared only using the same definition. This work also provides multiple climatologies that

358   can be used for evaluation and comparisons in the future with other models and observations

359   using similar definitions. Since the PBL depth in GEOS-5 is not purely diagnostic, but feeds

360   back on the turbulence through the turbulent length scale, the choice of definition is important

361   for vertical mixing and tracer transport. This aspect of the model will be evaluated in future

362   work.

363   Acknowledgments

366   References

367   Avissar, R. and R. A. Pielke (1989), A parameterization of heterogeneous land surfaces for

368   atmospheric numerical models and its impact on regional meteorology, Mon. Weather

369   Rev., 117, 2113-2136, doi: http://dx.doi.org/10.1175/1520-

370   0493(1989)117<2113:APOHLS>2.0.CO;2

371   Bacmeister, J. T., M. J. Suarez, and F. R. Robertson (2006), Rain Reevaporation, Boundary

372   Layer-Convection Interactions, and Pacific Rainfall Patterns in an AGCM, J. Atmos. Sci.,

373   63(12), 3383-3403, doi:10.1175/jas3791.1.

374   Beljaars, A. C. M. (1995), The impact of some aspects of the boundary layer scheme in the

375   ECMWF model, paper presented at ECMWF Seminar on Parameterization of Subgrid-

376   Scale Physical Processes, ECMWF, Reading, England.

377   Blackadar, A. K. (1962), The vertical distribution of wind and turbulent exchange in a neutral

378   atmosphere, J. Geophys. Res., 67(8), 3095-3102, doi:10.1029/JZ067i008p03095.

379   Chou, M.-D., and M. J. Suarez (1999), A solar radiation parameterization for atmospheric

380   studies, 40 pp., in Technical Report Series on Global Modeling and Data Assimilation,

381   edited by M. J. Suarez, NASA, Greenbelt, MD.

382   (http://gmao.gsfc.nasa.gov/pubs/docs/Chou136.pdf)

383   Chou, M.-D., M. J. Suarez, X.-Z. Liang, and M. M.-H. Yan (2001), A thermal infrared radiation

384   parameterization for atmospheric studies, 56 pp., in Technical Report Series on Global

385   Modeling and Data Assimilation, edited by M. J. Suarez, NASA, Greenbelt, MD.

386   (http://ntrs.nasa.gov/archive/nasa/casi.ntrs.nasa.gov/20010072848_2001122986.pdf)

387   Gurney, K., et al. (2002), Towards robust regional estimates of CO2 sources and sinks using

388   atmospheric transport models, Nature, 415(6872), 626-630, doi:10.1038/415626a.

389 Helfand, H. M., and S. D. Schubert (1995), Climatology of the Simulated Great Plains Low-
390   Level Jet and Its Contribution to the Continental Moisture Budget of the United States, J.
391   Climate, 8(4), 784-806, doi:10.1175/1520-0442(1995)008<0784:COTSGP>2.0.CO;2.

392 Holtslag, A. A. M., and B. A. Boville (1993), Local Versus Nonlocal Boundary-Layer Diffusion
393   in a Global Climate Model, J. Climate, 6(10), 1825-1842, doi:10.1175/1520-
394   0442(1993)006<1825:LVNBLD>2.0.CO;2.

395 Joffre, S. M., M. Kangas, M. Heikinheimo, and S. A. Kitaigorodskii (2001), Variability Of The
396   Stable And Unstable Atmospheric Boundary-Layer Height And Its Scales Over A Boreal
397   Forest, Bound.-Lay. Meteorol., 99(3), 429-450, doi:10.1023/a:1018956525605.

398 Koster, R. D., M. J. Suarez, A. Ducharne, M. Stieglitz, and P. Kumar (2000), A catchment-based
399   approach to modeling land surface processes in a general circulation model: 1. Model
400   structure, J Geophys Res-Atmos, 105(D20), 24809-24822, doi:10.1029/2000jd900327.

401 Lin, S.-J. (2004), A "Vertically Lagrangian" Finite-Volume Dynamical Core for Global Models,
402   Mon. Weather Rev., 132(10), 2293-2307, doi:10.1175/1520-
403   0493(2004)132<2293:AVLFDC>2.0.CO;2.

404 Lock, A. P., A. R. Brown, M. R. Bush, G. M. Martin, and R. N. B. Smith (2000), A New
405   Boundary Layer Mixing Scheme. Part I: Scheme Description and Single-Column Model
406   Tests, Mon. Weather Rev., 128(9), 3187-3199, doi:10.1175/1520-
407   0493(2000)128<3187:anblms>2.0.co;2.

408 Louis, J., M. Tiedtke, and J. Geleyn (1982), A short history of the PBL parameterization at
409   ECMWF, paper presented at Workshop on Planetary Boundary Layer Parameterization,
410   ECMWF, Reading, England.

411   McMahon, T. A., B. L. Finlayson, A. T. Haines, and R. Srikanthan (1992), Global Runoff -

412   Continental Comparisons of Annual Flows and Peak Discharges, 166 pp., Catena Verlag,

413   Cremlingen, Germany.

414   Molod, A., and H. Salmun (2002), A global assessment of the mosaic approach to modeling land

415   surface heterogeneity, J Geophys Res-Atmos, 107(D14), 26, doi:10.1029/2001jd000588.

416   Molod, A., L. Takacs, M. J. Suarez, J. T. Bacmeister, I.-S. Song, and A. Eichmann (2012), The

417   GEOS-5 Atmospheric General Circulation Model: Mean Climate and Development from

418   MERRA to Fortuna 115 pp., in Technical Report Series on Global Modeling and Data

419   Assimilation, edited by M. J. Suarez, NASA, Greenbelt, MD.

420   (http://ntrs.nasa.gov/archive/nasa/casi.ntrs.nasa.gov/20120011790_2012011404.pdf)

421   Moorthi, S., and M. J. Suarez (1992), Relaxed Arakawa-Schubert. A Parameterization of Moist

422   Convection for General Circulation Models, Mon. Weather Rev., 120(6), 978-1002,

423   doi:10.1175/1520-0493(1992)120<0978:rasapo>2.0.co;2.

424   Peel, M. C., T. A. McMahon, and B. L. Finlayson (2004), Continental differences in the

425   variability of annual runoff-update and reassessment, J Hydrol, 295(1-4), 185-197,

426   doi:10.1016/j.jhydrol.2004.03.004.

427   Peel, M. C., B. L. Finlayson, and T. A. McMahon (2007), Updated world map of the Köppen-

428   Geiger climate classification, Hydrol Earth Syst Sc, 11(5), 1633-1644.

429   Putman, W. M., and S.-J. Lin (2007), Finite-volume transport on various cubed-sphere grids, J.

430   Comput. Phys., 227(1), 55-78, doi: http://dx.doi.org/10.1016/j.jcp.2007.07.022.

431   Rienecker, M. M., et al. (2008), The GEOS-5 Data Assimilation System—Documentation of

432   Versions 5.0.1, 5.1.0, and 5.2.0 101pp., in Technical Report Series on Global Modeling

433   and Data Assimilation, edited by M. J. Suarez, NASA, Greenbelt, MD.

434   (http://gmao.gsfc.nasa.gov/pubs/docs/GEOS5_104606-Vol27.pdf)

435   Rienecker, M. M., et al. (2011), MERRA: NASA's Modern-Era Retrospective Analysis for

436   Research and Applications, J. Climate, 24(14), 3624-3648, doi:10.1175/jcli-d-11-

437   00015.1.

438   Seibert, P., F. Beyrich, S.-E. Gryning, S. Joffre, A. Rasmussen, and P. Tercier (2000), Review

439   and intercomparison of operational methods for the determination of the mixing height,

440   Atmos. Environ., 34(7), 1001-1027, doi:10.1016/s1352-2310(99)00349-0.

441   Seidel, D. J., C. O. Ao, and K. Li (2010), Estimating climatological planetary boundary layer

442   heights from radiosonde observations: Comparison of methods and uncertainty analysis,

443   J. Geophys. Res., 115(D16), D16113, doi:10.1029/2009jd013680.

444   Seidel, D. J., Y. Zhang, A. Beljaars, J.-C. Golaz, A. R. Jacobson, and B. Medeiros (2012),

445   Climatology of the planetary boundary layer over the continental United States and

446   Europe, J Geophys Res-Atmos, 117(D17106), doi:10.1029/2012jd018143.

447   Stull, R. B. (1988), An introduction to boundary layer meteorology, 666 pp., Kluwer Academic

448   Publishers, Norwell, MA.

449   Triantafyllou, G. N., and A. A. Tsonis (1994), Assessing the ability of the Köppen System to

450   delineate the general world pattern of climates, Geophys Res Lett, 21(25), 2809-2812,

451   doi:10.1029/94gl01992.

452   Vogelezang, D. H. P., and A. A. M. Holtslag (1996), Evaluation and model impacts of

453   alternative boundary-layer height formulations, Bound.-Lay. Meteorol., 81(3-4), 245-269,

454   doi:10.1007/bf02430331.

455   White, A. B., C. J. Senff, and R. M. Banta (1999), A Comparison of Mixing Depths Observed by

456   Ground-Based Wind Profilers and an Airborne Lidar, J. Atmos. Ocean. Tech., 16(5),

457   584-590, doi:10.1175/1520-0426(1999)016<0584:acomdo>2.0.co;2.

458

459   Figure 1 Köppen-Geiger climate classes as determined by *Peel et al.* [2007] regridded to the

460   0.5°x0.5° grid used by GEOS-5. The first letter indicates the broad climate class as tropical (A),

461   arid (B), temperate (C), cold (D), and polar (E).

462

463   Figure 2 Scatter plot of PBL depth versus sensible heat flux for the arid, hot desert climate class

464   in winter. Each dot represents the seasonal mean midday PBL depth and sensible heat flux. The

465   PBL depth is defined using the default scalar diffusivity definition in GEOS-5. The Australian

466   deserts are highlighted in color according to evaporative fraction.

467

468   Figure 3 Scatter plot of PBL depth versus 10-meter temperature for the tropical rainforest climate

469   class in the winter. Each dot represents the seasonal mean midday PBL depth and sensible heat

470   flux. The PBL depth is defined using the default scalar diffusivity definition in GEOS-5. The

471   colors highlight the relative humidity.

472

473   Figure 4 Seasonal mean diurnal cycle of PBL depth for climate classes Dsa (Cold with dry, hot

474   summers, during summer and winter, 4a and 4c) and BWh (hot, arid desert, during summer and

475   winter, 4b and 4d) using 7 different methods for estimating the PBL depth.

476

477   Figure 5 Seasonal mean diurnal cycle of PBL depth for climate classes Af (tropical rainforest)

478   during summer (5a) and winter (5b) using 7 different methods for estimating the PBL depth.
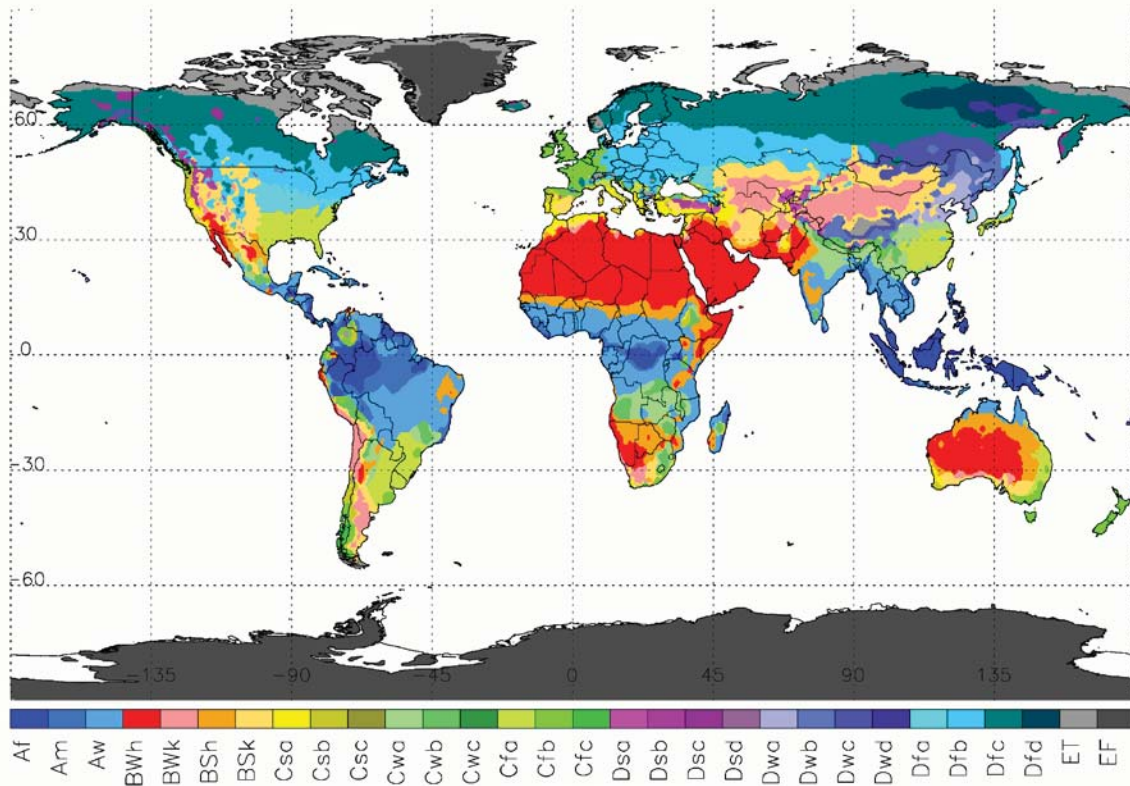
479

480   Figure 6 Seasonal mean vertical profile of total and Louis scalar diffusivities (6a) and bulk

481   Richardson number (6b) for JJA in the Amazonian rainforest. The dashed lines represent the

482   PBL depth as determined by method 1 (6a) and method 4 (6b).

483

484   Figure 7 Diurnal cycle of PBL depth response to radiative plumes during JJA. The figure shows

485   the scalar diffusivity method using a 10% of the column maximum threshold including the

486   radiative plume minus the same method, but without the radiative plume. Each subplot is

487   labeled   with   the   current   time   in   UTC.

488

Koppen–Geiger Classification Types

489

Figure 1 Köppen-Geiger climate classes as determined by *Peel et al.* [2007] regridded to the

0.5°x0.5° grid used by GEOS-5. The first letter indicates the broad climate class as tropical (A),
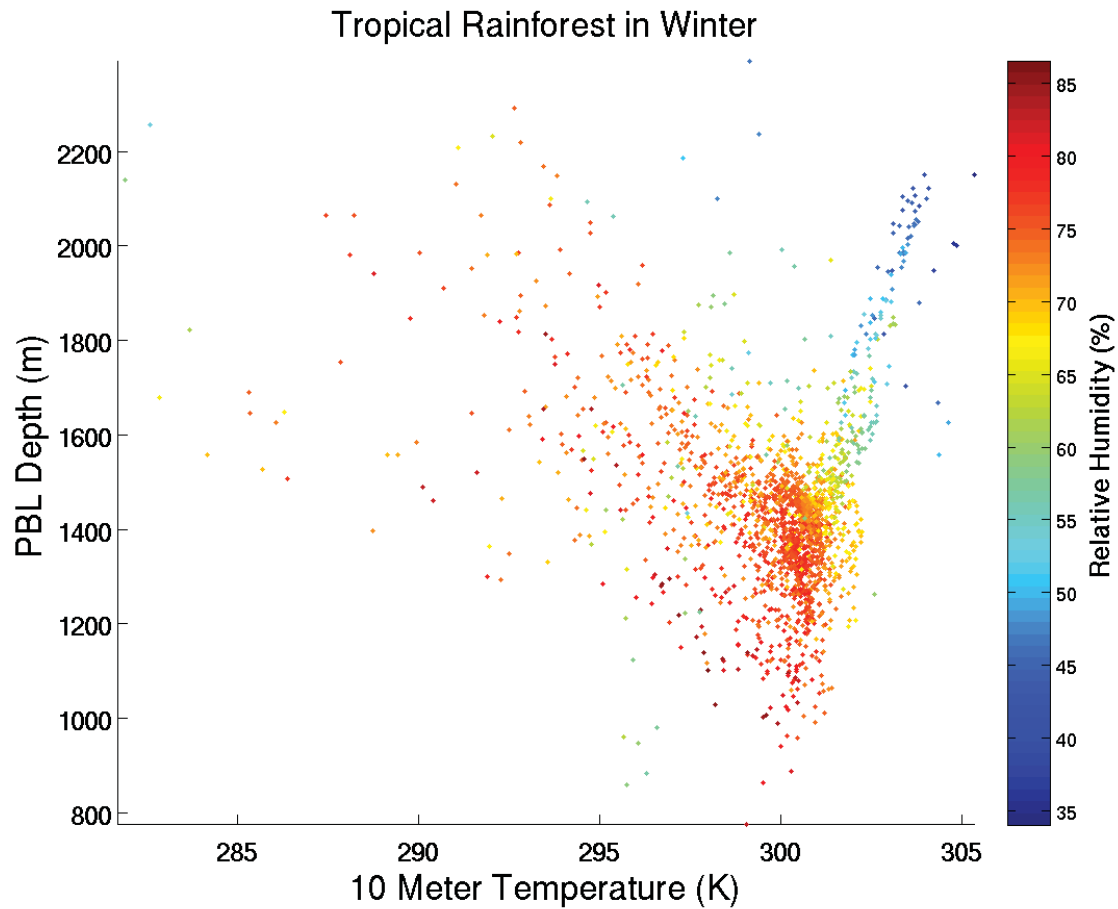
arid (B), temperate (C), cold (D), and polar (E).

493

Figure 2 Scatter plot of PBL depth versus sensible heat flux for the arid, hot desert climate class in winter. Each dot represents the seasonal mean midday PBL depth and sensible heat flux. The PBL depth is defined using the default scalar diffusivity definition in GEOS-5. The Australian deserts are highlighted in color according to evaporative fraction.
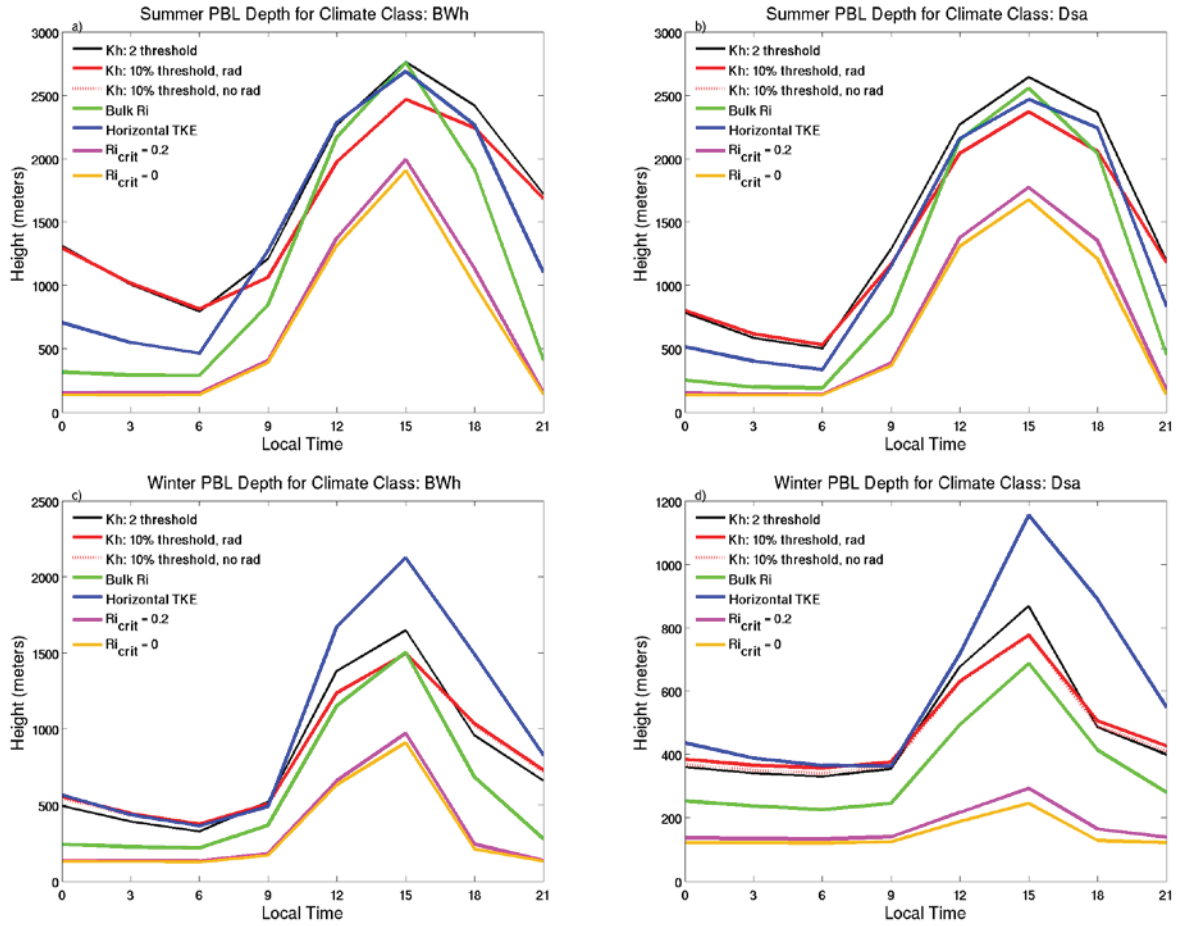
494

495

496

497

498

499

Figure 3 Scatter plot of PBL depth versus 10-meter temperature for the tropical rainforest climate class in the winter. Each dot represents the seasonal mean midday PBL depth and sensible heat flux. The PBL depth is defined using the default scalar diffusivity definition in GEOS-5. The colors highlight the relative humidity.
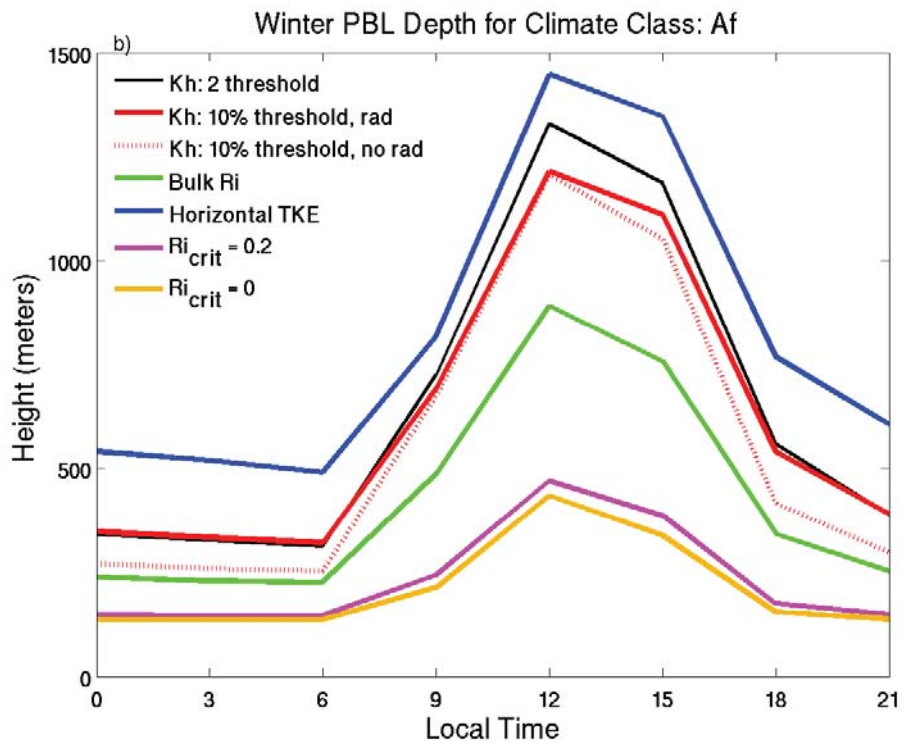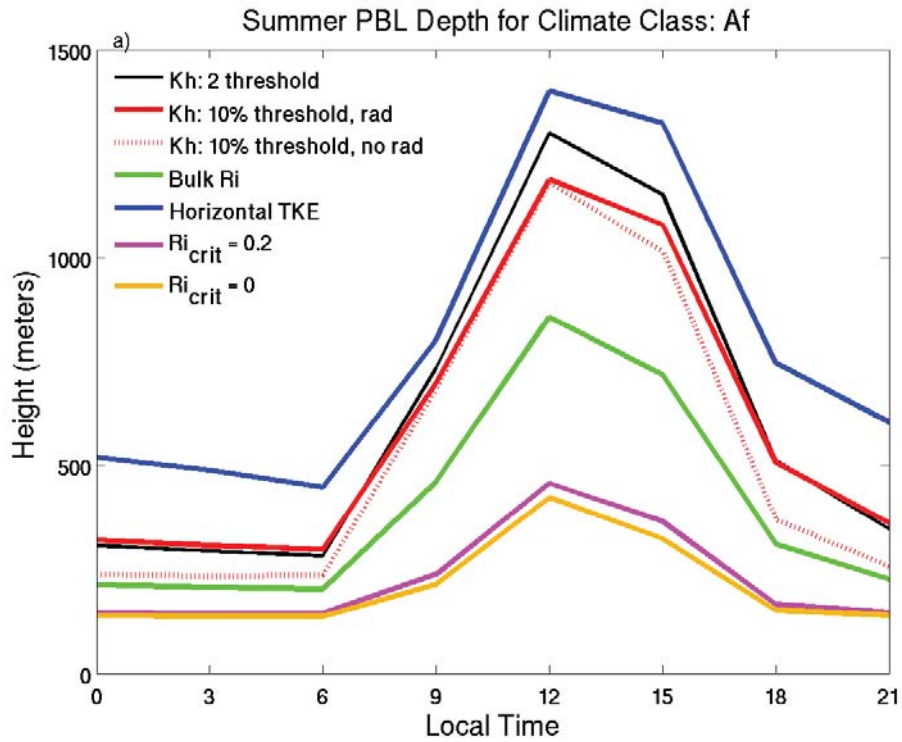
506

507   Figure 4 Seasonal mean diurnal cycle of PBL depth for climate classes Dsa (Cold with dry, hot

508   summers, during summer and winter, 4a and 4c) and BWh (hot, arid desert, during summer and

509   winter, 4b and 4d) using 7 different methods for estimating the PBL depth.
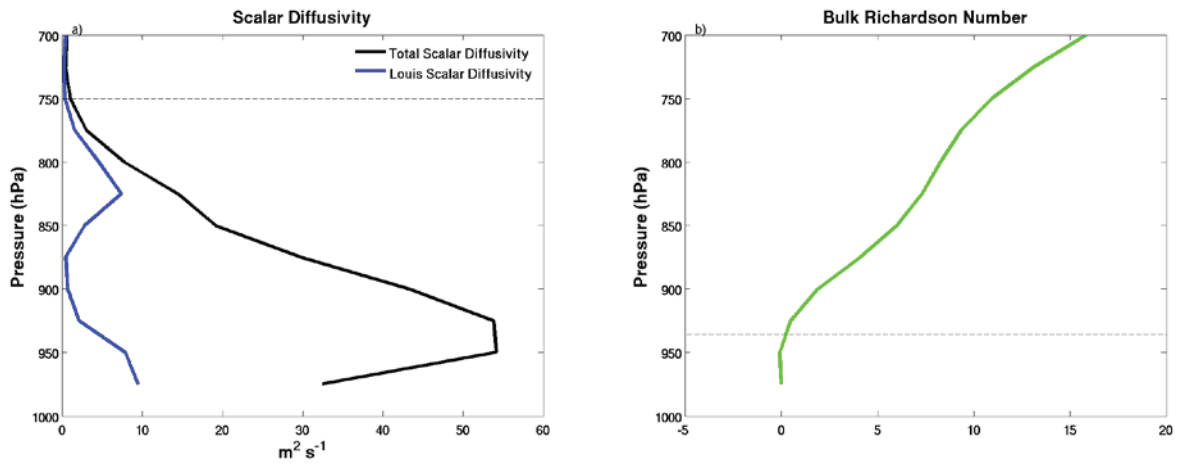
510

Figure 5 Seasonal mean diurnal cycle of PBL depth for climate classes Af (tropical rainforest) during summer (5a) and winter (5b) using 7 different methods for estimating the PBL depth.
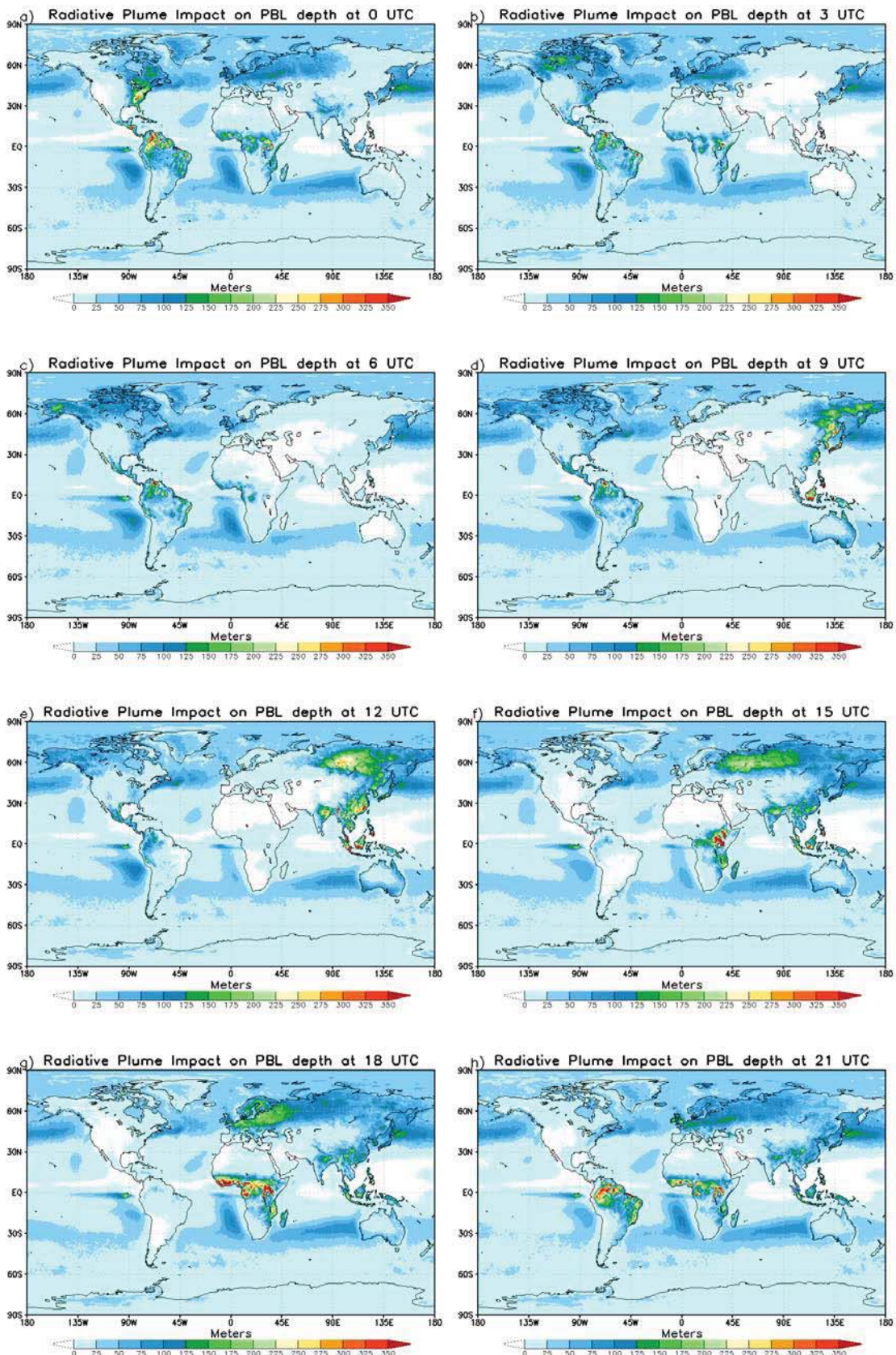
514

515

Figure 6 Seasonal mean vertical profile of total and Louis scalar diffusivities (6a) and bulk

Richardson number (6b) for JJA in the Amazonian rainforest. The dashed lines represent the

PBL depth as determined by method 1 (6a) and method 4 (6b).

519

a) Radiative Plume Impact on PBL depth at 0 UTC
b) Radiative Plume Impact on PBL depth at 3 UTC
c) Radiative Plume Impact on PBL depth at 6 UTC
d) Radiative Plume Impact on PBL depth at 9 UTC
e) Radiative Plume Impact on PBL depth at 12 UTC
f) Radiative Plume Impact on PBL depth at 15 UTC
g) Radiative Plume Impact on PBL depth at 18 UTC
h) Radiative Plume Impact on PBL depth at 21 UTC

520

521   Figure 7 Diurnal cycle of PBL depth response to radiative plumes during JJA. The figure shows

522   the scalar diffusivity method using a 10% of the column maximum threshold including the

523   radiative plume minus the same method, but without the radiative plume. Each subplot is

524   labeled   with   the   current   time   in   UTC.

525

526

527   Summary of PBL depth Methods

Method	Abbreviation	Description
1	Kh: 2 threshold	Uses total scalar diffusivity and a threshold of 2 $m^2\,s^{-1}$, this is the default PBL depth in GEOS-5
2	Kh: 10% threshold, rad	Uses total scalar diffusivity and a threshold equal to 10% of the column maximum, includes the radiative plume
3	Kh: 10% threshold, no rad	Uses total scalar diffusivity and a threshold equal to 10% of the column maximum, does not include the radiative plume
4	Bulk Ri	Uses the bulk Richardson number used by *Seidel et al.* [2012] and a critical value of 0.25
5	$Ri_{crit} = 0.2$	Uses a Richardson number and a critical value of 0.2
6	$Ri_{crit} = 0$	Uses a Richardson number and a critical value of 0
7	Horizontal TKE	Uses the diagnosed horizontal turbulent kinetic energy and a threshold of 10% of the column maximum

528

529   Table 1 List of the PBL depth methods used along with the abbreviations.